Available online at www.sciencedirect.com
ScienceDirect
Journal of the European Ceramic Society 31 (2011) 2601–2611
www.elsevier.com/locate/jeurceramsoc

Functional ceramic and nanocomposite fibers, cellular articles and microspheres via radiation curable colloidal dispersions

Yoram de Hazan [a,*], Veronika Märkl [a,b], Judit Heinecke [a,b], Christos Aneziris [b], Thomas Graule [a,b]

[a] *Laboratory for High Performance Ceramics, Empa, Swiss Federal Laboratories for Materials Science and Technology, Überlandstrasse 129, CH-8600 Dübendorf, Switzerland*

[b] *TU Freiberg, Institute of Ceramic, Glass and Construction Materials, D-09596 Freiberg, Germany*

Available online 3 January 2011

Abstract

We present here new cellular ceramics, fibers and microspheres produced by novel and general microshaping techniques employing colloidal dispersions in solvent free radiation curable monomer mixtures. High loading, low viscosity dispersions of functional nanoparticles such as TiO_2 and α-Fe_2O_3 and colloidal $Fe(C_2O_4)\cdot 2H_2O$ metal salt are achieved with comb-polyelectrolyte surfactants and/or mildly polar resins. TiO_2 dispersions are spun and solidified "on the fly" by UV radiation into continuous ceramic/polymer nanocomposite fibers with dimensions below 10 μm. $Fe(C_2O_4)\cdot 2H_2O$ dispersions provide a UV curable alternative to α-Fe_2O_3 dispersions which can only be thermally cured. The $Fe(C_2O_4)\cdot 2H_2O$ nanocomposites transform to α-Fe_2O_3 below 550 °C. Novel cellular Al_2O_3, TiO_2 and α-Fe_2O_3 articles with porosity >80% and precise replication of the pore-forming agents have also been produced from such dispersions. Al_2O_3 nanocomposite microspheres are produced by emulsification of the dispersions in an appropriate medium and UV curing.

Keywords: Fiber; Nanocomposite; Ceramic; Cellular; Microsphere; UV

1. Introduction

Radiation curable dispersions are frequently used for the fabrication of complex 3d articles layer-by-layer by employing lithographic techniques.[1–9] For these applications, reactive diluents and multifunctional monomers/oligomers are preferred in order to produce high quality interface between layers and strong crosslinked articles, respectively. No lower limit for feedstock viscosity essentially exists for these applications. However, resolution considerations and the requirement that the composites subsequently transform after debinding and sintering to crack free, dense inorganic materials imply that highly filled systems with particles in the colloidal range should be used. Therefore, the feedstock is used at or close to its higher viscosity limit, below ~5 Pa s (at 30 s^{-1}).[1,2] Similar considerations exist in gel and tape casting applications.

Recently, we have developed a new class of high loading/low viscosity radiation curable Al_2O_3, ZnO and mixed ZnO/Al_2O_3 colloidal dispersions which are suitable for stereolithography applications, relying on comb-polyelectrolyte surfactants.[10] Such UV curable dispersions have been used recently for the demonstration of new ceramic/polymer nanocomposite and nanoceramic fibers.[11,12] The dispersions are shaped by extrusion or draw processes and cured instantly 'on the fly' by UV radiation to continuous, solid nanocomposite fibers.

In this paper we first present new solvent free, radiation curable colloidal dispersions of functional particles such as $Fe(C_2O_4)\cdot 2H_2O$ metal salts, and comb-polyelectrolyte stabilized hematite (α-Fe_2O_3) and TiO_2 nanoparticles. These dispersions of functional particles can be used to create ceramic and ceramic/polymer nanocomposites thin films and microstructures and find applications in filtration, catalysis, sensing and detection, biomedicine, renewable energy and smart materials.

Second, we investigated the radiation curing of the dispersions and subsequent transformation of the cured nanocomposites to ceramics. Due to the high UV–vis absorption of the α-Fe_2O_3 nanoparticles, hematite dispersions cannot be solidified by medium intensity UV radiation. The TiO_2 and $Fe(C_2O_4)\cdot 2H_2O$ (iron oxalate dihydrate) dispersions are successfully spun and UV cured to produce TiO_2/polymer and $Fe(C_2O_4)\cdot 2H_2O$/polymer nanocomposite fibers.

* Corresponding author. Tel.: +41 0 44 823 4817; fax: +41 0 44 823 4150.
E-mail address: Yoram.dehazan@empa.ch (Y. de Hazan).

0955-2219/$ – see front matter © 2010 Elsevier Ltd. All rights reserved.
doi:10.1016/j.jeurceramsoc.2010.12.006

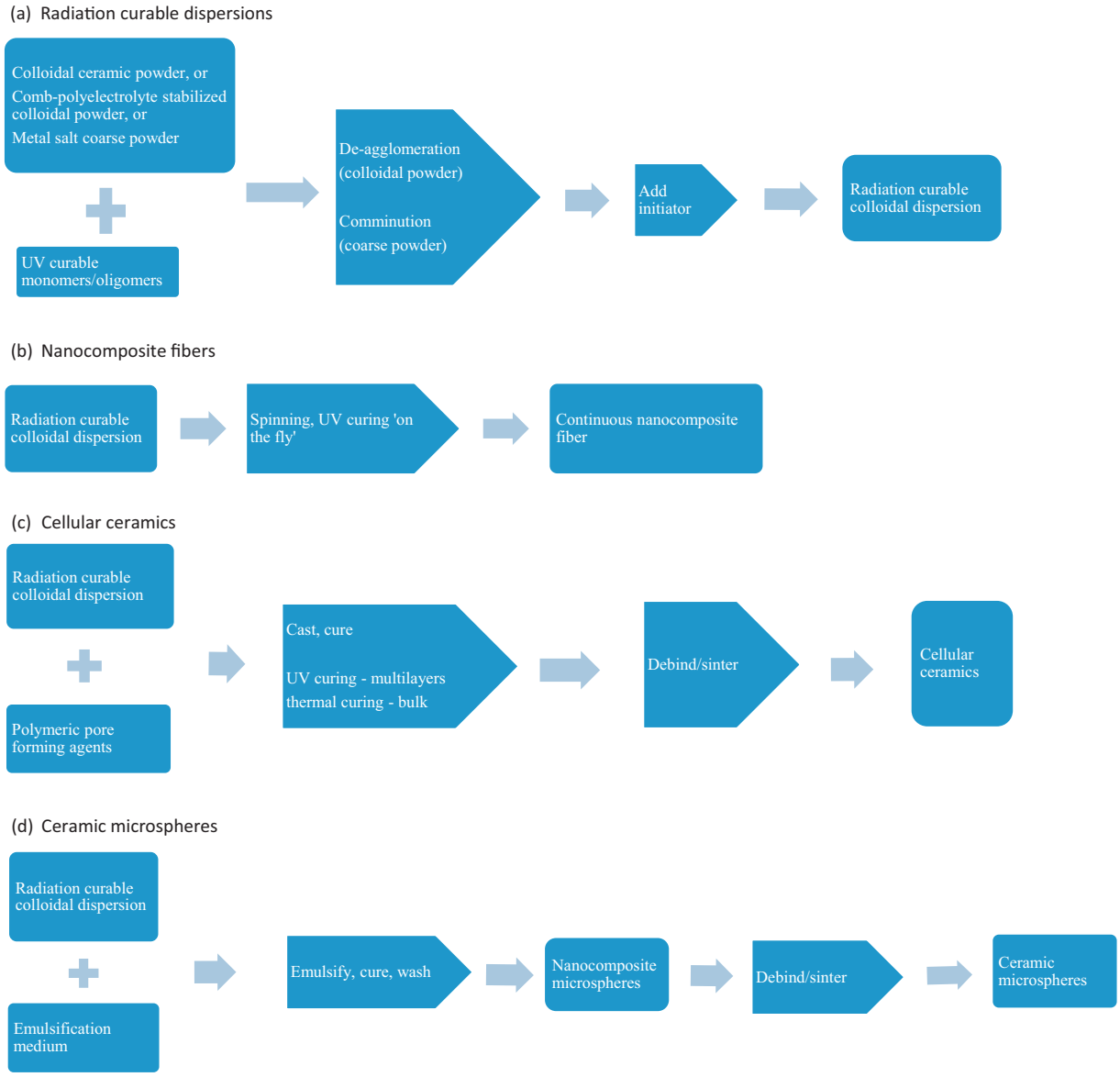

Fig. 1. Materials and microshaping procedures covered in the present study. (a) Types of radiation curable dispersions produced in this work and their use for the fabrication of (b) nanocomposite fibers, (c) cellular ceramics, and (d) ceramic microspheres.

Cellular materials find applications in thermal and acoustic insulation, catalysis and separation, light structures, biomedicine and renewable energy applications. Over the last decades, a few fabrication routes to cellular ceramics which are based on micro-templating of pre-polymer or colloidal based materials have been developed.[13–20] The micro-templating or pore forming agents may be added to the system as entities which are stable during the consolidation of the green body or generated/expand in situ.[14,18]

The next section of the paper presents Al_2O_3, TiO_2 and α-Fe_2O_3 cellular ceramic articles produced via a novel method which relies on the solvent free, high loaded/low viscosity radiation curable dispersions containing solid micro-templating agents.[21] The last section demonstrates new Al_2O_3 microspheres produced via emulsification of similar dispersions in suitable fluids, solidification by UV curing and standard debinding/sintering procedures.

The structure of the paper and the topics covered in this work are illustrated in Fig. 1. In the first section, the preparation of new radiation curable functional nanoparticle dispersions is presented (Fig. 1a). These dispersions, along with dispersions developed earlier[10,22] are used here to demonstrate new microshaping techniques where non-stable or metastable shapes are solidified by UV or thermal curing. Thus, in the second section, the transformation of such functional dispersions to nanocomposite fibers is shown (Fig. 1b). The third section reports for the first time cellular ceramics derived from curable dispersions containing polymeric pore forming agents (Fig. 1c). Here, the possibility of using metal salts colloidal dispersions is also demonstrated. And last, the fabrication of nanocomposite and ceramic microspheres using new emulsification based processes is illustrated (Fig. 1d).

2. Experimental

2.1. Materials

Table 1 presents the manufacturer, specific surface area and particle size (as provided by manufacturer) of the powders used in the study. The surface area was determined by the BET method with a SA3100 (Beckman Coulter, USA). The powders were treated for 2 h with N_2 at 180 °C to remove adsorbed water. Note that this treatment may also partially dehydrate the $Fe(C_2O_4)\cdot 2H_2O$ salt. SiO_2 (Aerosil OX50) is amorphous and TiO_2 (Aeroxide P25) consists of 80% anatase/20% rutile. α-Al_2O_3 and α-Fe_2O_3 denotes the corundum and hematite phases, respectively. The purity of the $Fe(C_2O_4)\cdot 2H_2O$ salt used is 99%.

The surfactant used is a commercial comb-polyelectrolyte surfactant (Melpers4343) from BASF, Germany.[10] The UV curable monomers used in this study are 2-hydroxy ethyl acrylate (2-HEA), 4-hydroxy butyl acrylate (4-HBA) from BASF, Germany and polyethylene glycol 200 diacrylate (PEGDA) from Rahn, Switzerland. The chemical structure of the monomers and photoinitiator (LTM, described below) was reported for example by Wozniak et al.[22] The UV curable mixture contains either 2-HEA/PEGDA (for Al_2O_3 cellular materials and microspheres and SiO_2 fibers) or 4-HBA/PEGDA (for all other fibers and cellular materials). In both cases the ratio monoacrylate/diacrylate was 14:1. The monomer mixture is used without any additional solvents/diluents. A commercial UV curable resin used for rapid prototyping applications was used for comparison. Genocure LTM, a liquid photoinitiator blend with a broad absorption peak around 380 nm from Rahn, Switzerland was used as the photoinitiator. Azobisisobutyronitrile (AIBN, Sigma Aldrich, 98%) was used as a thermal initiator.

Pore forming agents were polyethylene (PE) microspheres (Sumitomo, Japan) with an average diameter of 12 μm and a broad size distribution (3–25 μm), and 40 μm polystyrene (PS) or 10 μm polymethyl methacrylate (PMMA) microspheres (Microbeads, Norway) with a narrow size distribution.

Glycerol (Sigma Aldrich, 99.5%) was used as a dynamic sheathing liquid for extrusion. Mazolla corn oil (Coop, Switzerland) was used as an emulsifying medium for the preparation of microspheres.

2.2. Dispersion preparation and characterization

SiO_2 and $Fe(C_2O_4)\cdot 2H_2O$ powders were used as received, without surfactants. Dispersions of SiO_2 (30 vol%) in UV curable monomer mixtures were prepared with the aid of a laboratory dissolver (Ultra Turrax T 50, USA)) by a procedure described elsewhere in detail.[22] Dispersions of $Fe(C_2O_4)\cdot 2H_2O$ (32 vol%) in 4-HBA/PEGDA (14:1) or a commercial resin (Objet Geometries, Israel) were prepared by milling the powders in the monomer mixture with 3 mm and 10 mm ZrO_2 balls in a planetary ball mill (PM400, Retch, Inc., Germany) at 250 rpm for 30 min.

Nanopowders with adsorbed surfactants were produced by the procedure described previously in detail.[10] In short, the water soluble surfactants are added to an electrostatically stable aqueous nanoparticle dispersion. The dispersion is deflocculated, aged, centrifuged, decanted and the deposit dried in an oven at 55 °C and ground to a coarse powder with adsorbed surfactants before dispersion in the monomer.

Zeta potential measurements were used to determine the isoelectric point of the powders by potentiometric titrations of 2.5–5% dispersions by the electroacoustic method (Zetaprobe, Colloidal dynamics, Australia). The dispersions were first titrated from their natural pH in DI water to pH 10–11 (first leg) followed by titration to the pH range of 3–4 (second leg). The IEP is reported for the second leg (Table 2). Optimal surfactant concentrations were determined by zeta potential measurements made during titrations of 5% dispersions with a 7.5% aqueous surfactant solution.[10] Table 2 summarizes the aqueous dispersion characteristics and the surfactant concentration added to the dispersions.

Dispersions of Al_2O_3 (41.5 vol%), TiO_2 (17 vol%) and α-Fe_2O_3 (19 vol%) were prepared by dispersing the powders with adsorbed comb-polyelectrolyte surfactants in the UV curable monomer mixtures with the milling procedure described above for $Fe(C_2O_4)\cdot 2H_2O$ followed by 2–4 min ultrasonication.

Table 1
Nanoparticles used in this study.

Nanopowder	Manufacturer	Specific surface area (m^2/g)	Particle size (nm)
α-Al_2O_3	Taimei Chemical, Japan	12.5	120
TiO_2	Evonic Degussa, Germany	49	25
SiO_2	Evonic Degussa, Germany	50	40
α-Fe_2O_3	NanoAmor, USA	24	20–30
$Fe(C_2O_4)\cdot 2H_2O$	Sigma Aldrich, Switzerland	35	n/a

Table 2
Characteristics of the aqueous nanoparticle dispersions used.

Materials	Natural pH/zeta potential (mV)	Isoelectric point	Surfactant added (per particle weight) (%)	Minimum–maximum amount of surfactant (per particle weight) (%)
TiO_2	3/79.5	5.9	10	4.4–5.6
α-Fe_2O_3	6.8/17	8.6	15	5.1–7.1

Pastes for cellular materials were prepared by mixing the dry pore formers into the above dispersions in an amount of 50–83% equivalent porosity. The equivalent porosity, which is an estimate for the porosity of the final cellular material, is defined by the following equation: equivalent porosity = 100 Vpf/(Vpf + Vp), where Vpf and Vp are the volumes of pore formers and inorganic particles, respectively.

A liquid photoinitiator (LTM, Rahn, Switzerland) in an amount of 3–5% or the thermal initiator (AIBN) in an amount of 0.5–1% (both calculated per monomer mixture) were added to the dispersions or pastes and mixed thoroughly. Dispersions and pastes containing AIBN were used shortly after the addition of the initiator. Dispersions or pastes containing the photoinitiator were kept in containers covered with aluminum foil until use.

The particle size distribution (PSD) was measured with a Beckman Coulter LS230 (USA) equipped with polarization intensity differential scattering (PIDS) for reliable analysis in the submicron range. Aqueous dispersions with or without added surfactants were measured in DI water (pH ~5). The dispersions in monomer were first diluted with DI water and then measured in a similar fashion. The PSD of the dispersions was monitored during the different dispersion steps. The PSD found for electrostatically stable dispersions in aqueous media was used as a reference for a well dispersed system. Only dispersions with PSD essentially similar to the reference are reported.

Rheological measurements were performed with a rotational viscosimeter (Rheolab MC 120, PhysicaMesstechnik GmbH). Measurements were conducted at temperatures of 10, 23, 30 and 40 °C. 30 min were allowed for temperature stabilization before each measurement. The cylinder system (one gap and double-gap-system) were used depending on the viscosity of the dispersions. Homogenization of the dispersion at 10 s^{-1} for 3 min is done before each measurement. The measurement is repeated three times and consists of 20 measurement points from 10 to 1000 s^{-1} with a logarithmic progression of shear rate. Values from the last measurement (which was essentially similar to the second measurement) are reported. No thixotropy is observed in any of the dispersions. The viscosity of the SiO_2 dispersion is 0.8 Pa s (23 °C, 100 s^{-1}).[22]

2.3. Microshaping procedures, debinding and sintering

The extrusion system consists of 8 ml stainless steel syringe (Hamilton, USA) equipped with an exit die. The syringe which contains the UV curable dispersion is driven by a precision syringe pump (PHD 2000, Harvard Scientific, USA). Spinning dies were 9.5 mm luer-lock needles with diameters of 160, 340 and 500 μm (Hamilton, USA). The dispersions were extruded or co-extruded with a sheathing fluid through the various dies into a glass beaker with a diameter of 15 cm filled with DI water to a level of 15 cm. The exit die was positioned 1–3 cm inside the DI water and was shielded from UV radiation by an aluminum tape. The average linear velocity of the dispersion stream passing the die was varied in the range of 1–20 cm s^{-1}. A UV lamp producing 120 mW cm^{-2} in the UVA (Fe bulb, 100 W, Dr. Hönle AG, Germany)[12] positioned outside the beaker, illuminated the bottom 10 cm of the beaker and cured the dispersion stream 1–2 s after exiting the die. The continuous fibers such produced were separated from the water, washed with fresh water and dried. All materials (e.g., dispersions, sheaths) and all manipulations (e.g., curing and washing) were carried out at 25 °C.

The die delivering the dispersion for co-extrusion (hydrodynamic tensioning) of Al_2O_3 and TiO_2 dispersions consisted of a 160 μm needle (310 μm OD) concentrically positioned within a 500 μm tube delivering glycerol in the annular gap. The streams were combined 3–5 mm before exiting the die. The glycerol average linear velocity in the annular gap was fixed to 150 cm s^{-1} (0.13 cm^3 s^{-1}), corresponding to a Reynolds number of 0.3. A similar arrangement with larger die assembly was used for the $Fe(C_2O_4)\cdot 2H_2O$ based dispersions. 340 μm ID needle (600 μm OD) concentrically positioned within a 3 mm tube delivering glycerol in the annular gap.

Cellular Al_2O_3 fibers were produced from pastes containing pore formers by UV spinning through a 500 μm die as described above. Cellular disks were prepared by casting the pastes in a 2 cm diameter circular mold to 1–2 mm followed by curing of the sample from both sides. Homogeneous multilayered Al_2O_3 composites containing pore formers (27 vol% Al_2O_3, 83% equivalent porosity) were prepared by layering and curing layers of about 1000 μm, one on top of the other in a 2 cm diameter circular mold. The final thickness of the sample was about 10 mm. Curing of each layer for 1 min was done with the UV lamp described above integrated into a UV cube (UVCube100, Dr. Hönle AG, Germany).[10,22] Thin sheets (100–500 μm) were prepared by casting TiO_2 and $Fe(C_2O_4)\cdot 2H_2O$ pastes between two polypropylene foils and UV curing for 1 min from each side. Pastes of α-Fe_2O_3 dispersions containing pore formers were cast in 1 cm^3 molds and then thermally cured for 15–30 min in an oven at 85–90 °C.

Al_2O_3/polyacrylate microspheres were prepared by emulsifying a 41.5% Al_2O_3 dispersion with Mazolla oil followed by UV curing of the dispersion droplets in the emulsion obtained. The solid composite microspheres were separated from the emulsion, washed with isopropyl alcohol and water and dried before debinding and sintering procedures.

Debinding of composite fibers, cellular materials and microspheres was carried out in air at 650 °C for 2 h (Al_2O_3, SiO_2) or 550 °C (α-Fe_2O_3, TiO_2 and $Fe(C_2O_4)\cdot 2H_2O$). The pore formers are removed during the debinding step. SiO_2 fibers were sintered at 1250 °C for 1 h and quenched rapidly to 800 °C. Al_2O_3 fibers, microspheres and cellular articles were sintered at 1500 °C for 2 h followed by 15 h cooling to room temperature.

2.4. Material characterization

Thermogravimetric analysis (TGA/DTA 851, Mettler-Toledo) of the raw powders, powders with adsorbed surfactants and cured green bodies was performed in order to assess the amount of surfactant adsorbed and/or thermal decomposition of the $Fe(C_2O_4)\cdot 2H_2O$ powder and polymer formed during curing. The TGA heating profile consists in all cases of a 5 °C/min ramp and a 30-min soak at 100 °C to remove weakly adsorbed water molecules followed by a 5 °C/min ramp to 850 °C. Results were normalized to the weight of samples after the soak at 100 °C.

Ceramic and ceramic/polymer composite fibers were characterized by optical microscopy (Leica Wild M3Z equipped with micrometer) and SEM (VEGA Plus 5136 MM, Tescan instruments, Czech republic).

Mercury intrusion porosimetry (MIP, Pascal 140/440, Porotec GmbH, Germany) was used up to a pressure of 2000 bar for the determination of apparent and skeletal density, open and closed porosity and pore size distribution in the range of 4 nm −100 μm.

X-ray diffraction (XRD) of the materials was conducted with a Panalytical XPertPro diffractometer in the range $20^\circ \leq 2\Theta \leq 80^\circ$ using a scanning rate of $0.088^\circ\ min^{-1}$.

3. Results and discussion

3.1. Development of radiation curable TiO_2, α-Fe_2O_3 and $Fe(C_2O_4)\cdot 2H_2O$ colloidal dispersions

In this work we pre-stabilize the functional TiO_2 and α-Fe_2O_3 nanoparticles with comb-polyelectrolyte surfactants prior to their dispersion in UV curable media. Such procedure was developed previously for Al_2O_3 and ZnO.[10] The pre-stabilization step is carried out in an aqueous media. The nominal surfactant concentration (per particle weight) added to the aqueous dispersion is reported in Table 2. The stabilized particles are centrifuged, separated and dried before dispersion in the organic monomer medium. Such procedure removes soluble counter ions and excess surfactant.[10] The last column in Table 2 lists the minimum and maximum amount of surfactant (per particle weight) estimated by TGA measurements. The minimum and maximum values are obtained assuming no or full replacement of the surface hydroxyls in the original powders.[23] Surface hydroxyl content determined by TGA can be as high as to 1.5% (α-Fe_2O_3). The minimum and maximum surfactant amount is estimated to be between 34% and 56% of the nominal surfactant amount added to the system, respectively. This shows that excess surfactant is readily removed by centrifugation and that no free surfactant is likely to be transferred to the UV curable media.

Fig. 2 shows the viscosity of the stabilized functional nanoparticle dispersions in 4-HBA/PEGDA (14:1) monomer mixture. The dispersions, which have solid loadings in the 17–19 vol% range show almost Newtonian behavior at 23 °C and shear rates between 10 and 1000 s^{-1}, with viscosity below 0.3 Pa s (Fig. 2a). Most notably, the viscosity of the 19 vol% α-Fe_2O_3 is only ∼0.05 Pa s. Fig. 2b presents the relative viscosity of the dispersions in the 10–40 °C temperature range. The constant values indicate that the change of viscosity with temperature is dictated only by the monomer mixtures. In this temperature range the viscosity of the monomer mixtures varies between 5.6 and 17 mPas. It is important to mention that the processing of a nanoparticle such as TiO_2 through the route described above is not necessarily trivial due to risk of reactivity with the surfactant and monomers. Similar issues were observed previously with CeO_2 nanoparticles.[10] However, high quality dispersions are consistently produced when special care was taken during processing to avoid overheating and overexposure to light.

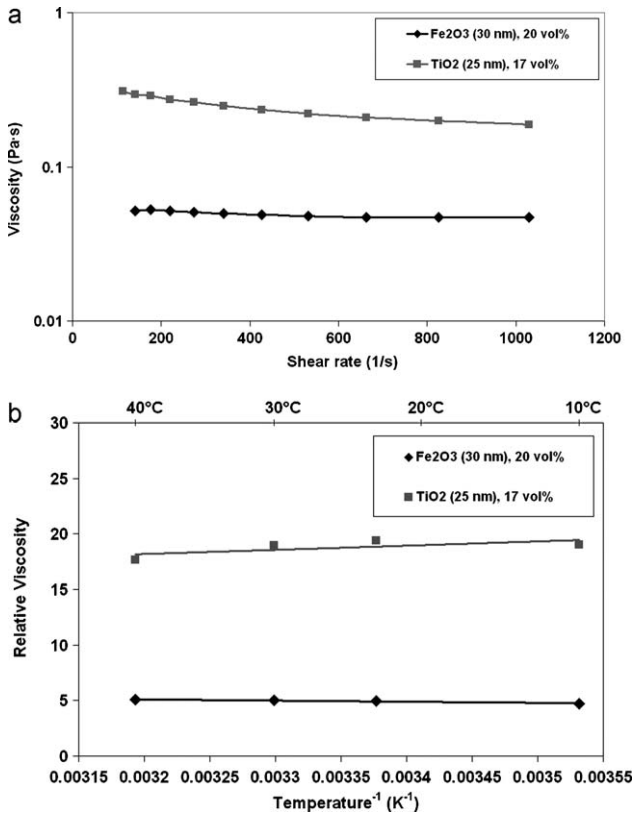

Fig. 2. Viscosity of comb-polyelectrolyte stabilized nanoparticle dispersions in 14:1 4-HBA/PEGDA UV curable monomer mixtures. (a) viscosity as a function of shear rate at 23 °C, (b) relative viscosity as a function of temperature (at 531 s^{-1}).

The UV curable organic media is also interesting for shaping of metal salts in their colloidal form. As will become apparent in Section 3.2, $Fe(C_2O_4)\cdot 2H_2O$ dispersions provide a UV curable alternative route to produce α-Fe_2O_3 fibers. Unlike the comb-polyelectrolyte stabilized dispersions described above, the $Fe(C_2O_4)\cdot 2H_2O$ dispersions/suspensions are prepared by milling the as-received coarse powder to finer powder directly in the resin, without added surfactants (Section 2.2). The milling of the $Fe(C_2O_4)\cdot 2H_2O$ powder proceeds quite differently in the two resins tested. PSD measurements reveal that the average particle size after milling is 1 μm in the 4-HBA/PEGDA (14:1) monomer mixture compared to 6 μm in the commercial resin. This may be related to differences in the resin composition but more likely to the viscosity of the media. The viscosity of the 4-HBA/PEGDA monomer mixture at 23 °C is 7.6 mPas compared to a value of ∼0.6 Pa s for the commercial resin. Fig. 3 shows 32 vol% $Fe(C_2O_4)\cdot 2H_2O$ dispersions in the two UV curable resins. Also here, relatively high loaded dispersions with viscosity well below 1 Pa s are achieved. This has different origin for the two cases. Due to the relatively large particle size (6 μm) the viscosity of the 32 vol% $Fe(C_2O_4)\cdot 2H_2O$ in the commercial resin is dominated by the resin itself (relative viscosity ∼1) whereas that of the somewhat smaller (1 μm) 32 vol% $Fe(C_2O_4)\cdot 2H_2O$ has a temperature independent relative viscosity of ∼5 and benefits from the low viscosity of the monomer mixture.

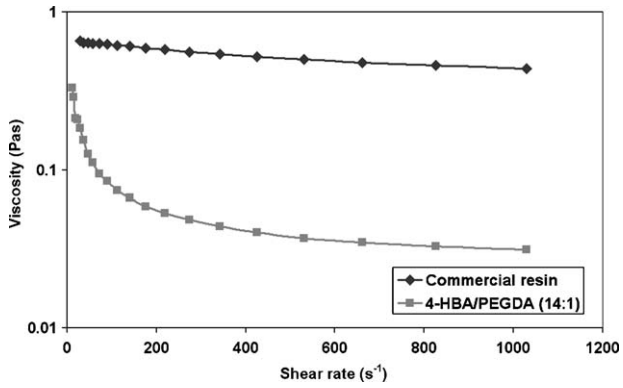

Fig. 3. Viscosity of 32 vol% $Fe(C_2O_4)\cdot 2H_2O$ dispersions in 14:1 4-HBA/PEGDA and a commercial UV curable resin.

3.2. Fabrication of TiO_2 and $Fe(C_2O_4)\cdot 2H_2O$ nanocomposite fibers

The use of UV curable dispersions for extrusion/spinning processes allows much more flexibility than in conventional spinning technologies. A detailed discussion about the new spinning concepts and UV curing 'on the fly' can be found in an earlier work.[12]

Fig. 4 presents the general scheme used here to produce functional inorganic/polymer nanocomposites. A curable colloidal dispersion is shaped into a thin filament through an extrusion/spinning die. The filament exiting the die is exposed to UV radiation which initiates photopolymerization of the monomer phase and hardens the material to a solid fiber shortly after exiting the die. The product of this spinning process is a new ceramic/polymer nanocomposite fiber. Such 'on the fly' curing scheme have recently been introduced for non-filled, organic polymer materials.[24] Dispersions exhibiting high surface tension and low viscosity are frequently prone to flow instabilities when forced at low flow rates through small orifices directly to air. These instabilities can be minimized or avoided altogether if extrusion is carried out into higher viscosity static or dynamic liquids such as water (Fig. 4). In the present work water is used as the static fluid and glycerol as (an optional) dynamic fluid. The dynamic sheathing fluid provides means for tensioning/elongation of the relatively low viscosity extruded filament,[12,24,25] and reduce the cross section of the filament. This in turn results in a proportional increase in fiber velocity and need for faster curing.

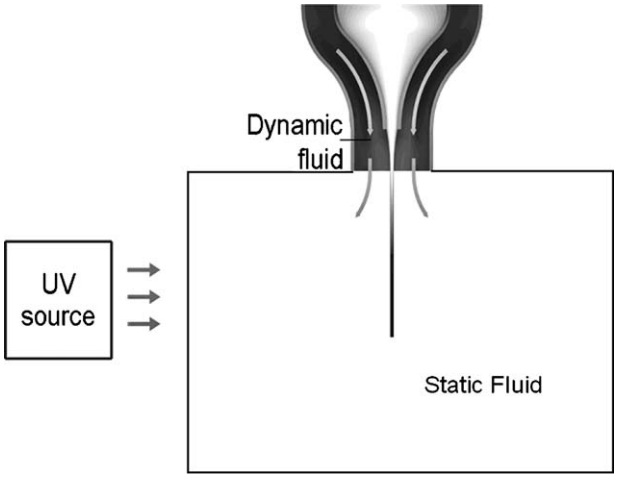

Fig. 4. Fabrication scheme for inorganic/polymer nanocomposite fibers.

For a given resin and photoinitiator system, the curing of UV curable colloidal dispersions is limited by scattering produced by the particles, the UV–vis intensity and spectrum, and the exposure time.[26,27] As discussed previously, the time spent in the radiation zone is short and limited for fibers solidified 'on the fly'. An important consideration is the absorption of radiation by the nanoparticles. We find that the spinning method of Fig. 4 works well when the nanoparticles in the dispersions show little absorption in the UV–vis spectrum. Fig. 5a shows an example of 30 vol% SiO_2/polyacrylate fibers extruded directly to water without a dynamic sheathing fluid. Due to the high transparency of the SiO_2 dispersion[22] fibers with diameters ~500 μm can be easily produced.

On the other hand, dispersions of semiconducting nanoparticles such as ZnO and TiO_2 should be inherently difficult to process with the new spinning concepts, since these nanoparticles block all UV radiation below 390–400 nm (hence their use in sunscreens).

In a previous publication we have demonstrated that films of ZnO colloidal dispersions with thickness ~100 μm can be cured with the use of a UV–vis source and a photoinitiator both acting in the near visible spectrum (<430 nm).[10] Fig. 5b and c shows optical and SEM micrographs, respectively, of 17 vol% TiO_2/polyacrylate fibers produced with the method of Fig. 4 using glycerol as a dynamic sheathing fluid. The fibers show dimensions between 5 and 40 μm. Part of this variation is related to the fact that the flow of dispersion was controlled manually. A closer inspection of the debinded fibers (Fig. 5c) reveals that fibers having circular cross section can be produced but the majority of fibers are in actuality microbelts having a width of 5–40 μm and thickness of ~2 μm. Fig. 5b, which shows that the large ~60 μm fibers are transparent is also consistent with a belt shape morphology. The reason for this phenomenon is not clear at the moment. It is likely that such structures are related to the properties of the glycerol sheathing fluid (relatively high viscosity and/or surface tension). Preliminary results have shown that the photocatalytic activity of the TiO_2/polyacrylate fibers for the degradation of methylene blue is only slightly lower than that of the non-modified nanoparticles.

Hematite (α-Fe_2O_3) nanoparticles, on the other hand, absorb strongly radiation in the UV–vis spectrum.[28] Curing of 19 vol% α-Fe_2O_3 dispersions to thin solid films was not possible with our medium intensity UV lamps employed in this study. The curing of the dispersions can be done thermally using appropriate thermal initiators such as peroxides[8] or Azo compounds as discussed in the next section. At the same time, UV curing of the dispersions is desirable since it enables operating the new spinning process at low temperatures with very short and controllable curing times. These may be advantageous for example for biological applications.[24] In addition, UV curing implies lithographic techniques can be employed to further produce complex microstructures by selective curing.

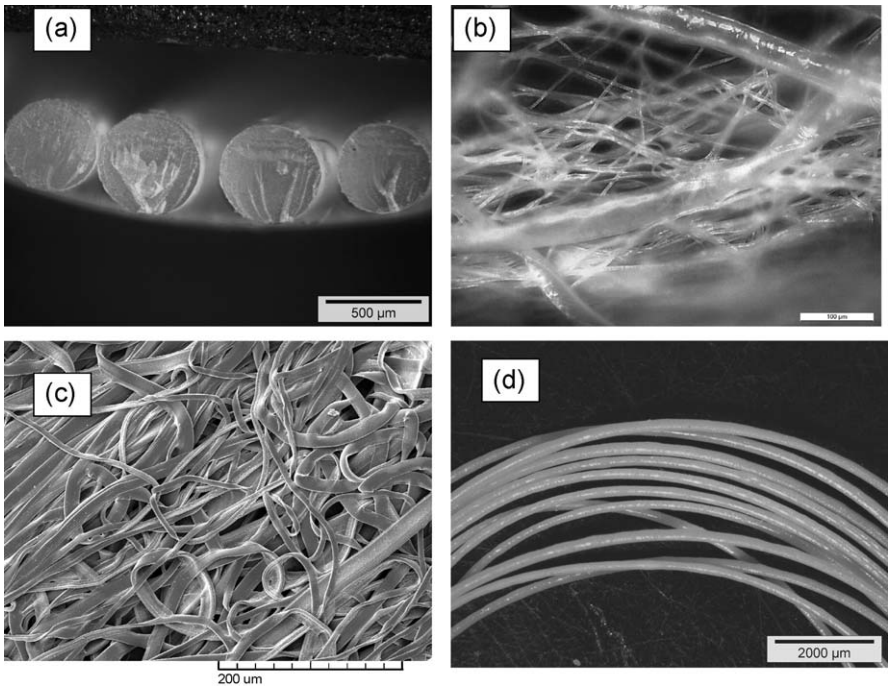

Fig. 5. Composite fibers produced from UV curable dispersions by the microshaping process of Fig. 4 using water as static fluid and glycerol as an optional dynamic fluid. (a) 30 vol% SiO_2/polyacrylate produced using only water as static fluid, (b) optical micrograph of 17 vol% TiO_2/polyacrylate, (c) SEM of 17 vol% TiO_2/polyacrylate, (d) 32 vol% $Fe(C_2O_4)\cdot 2H_2O$/commercial resin.

One of the interesting aspects of the new method is the ability to use organic media where metal salts can be processed as colloidal entities. Iron oxalate dihydrate, $Fe(C_2O_4)\cdot 2H_2O$, is transformed to hematite nanoparticles upon heating to temperatures above 250 °C in air.[29] The relatively low radiation absorption of $Fe(C_2O_4)\cdot 2H_2O$ based dispersions enables their spinning and rapid UV curing. Fig. 5d shows an example of a 32 vol% $Fe(C_2O_4)\cdot 2H_2O$/polymer fibers produced by the method of Fig. 4 using glycerol as a dynamic sheathing fluid. The fibers produced with the commercial resin show an average size of ~150 μm and quite circular cross section. In comparison, the fibers produced with 4-HBA/PEGDA monomer mixture have similar dimensions but are belt shaped. This result suggests that the retention of the circular shape of the fibers is potentially influenced by the higher viscosity or the composition of the commercial resin. The composite fibers produced with both resins transform to α-Fe_2O_3 below 550 °C as discussed in the next section.

3.3. Fabrication of Al_2O_3, TiO_2 and α-Fe_2O_3 cellular materials

We find that a high amount of pore formers such as gases, liquids or solids can be introduced into the solvent free, low viscosity dispersions. These UV curable pastes can be conveniently shaped and cured into fibers or multilayers and subsequently be transformed into high quality cellular ceramic articles. While larger, homogeneous cellular bodies are preferably thermally cured with the use of small amount of an appropriate thermal initiator, heterogeneous multilayer articles and fibers are preferably processed rapidly by UV–vis curing. One of the differences from other gel casting related technologies[13,14,17,18] is the ability to use compositions with reactive diluents (along with solid pore formers) which are cured to 100% solids. This system is common and ideal for layer-by-layer processing since a layer with good interface properties is formed instantly. The drying stage inherent with most casting/molding feedstock is absent and rewetting of cured layers by solvent or liquid pore formers does not occur. At the same time, the amount of organic matter in such systems is much higher in comparison to conventional gel casting systems. This complicates the debinding stage and may set new requirements for the binder system.

Fig. 6 shows several examples of cellular materials produced with the UV curable dispersions described above. Fig. 6a shows a broken section of a 79% porous cellular Al_2O_3 material prepared using PE pore former with an average size of 12 μm and a broad sphere size distribution (3–25 μm). It can be seen that the shape of the pore former is precisely replicated in the final ceramic article. The size distribution and final porosity can be predicted from the original size of pore formers and their relative volume per inorganic particles, respectively. In Fig. 6a most of the 10 μm cells are interconnected through 1–3 μm passages. MIP measurements show that 13.5% of the porosity, however, is impermeable to Hg. The average pore size found by MIP measurements is about 2 μm, corresponding closely to the passage between the cells seen in Fig. 6a. It can also be seen that the cell wall thickness is below 500 nm in many instances, corresponding to the size of only 2–3,150 nm particles (Fig. 6a, insert). This retention of fine structure may be aided by the crosslinked nature of the UV cured nanocomposite green bodies. Such benefit of crosslinking was shown previously for gel derived cellular materials.[17,18] The crosslinking degree, which can be promoted

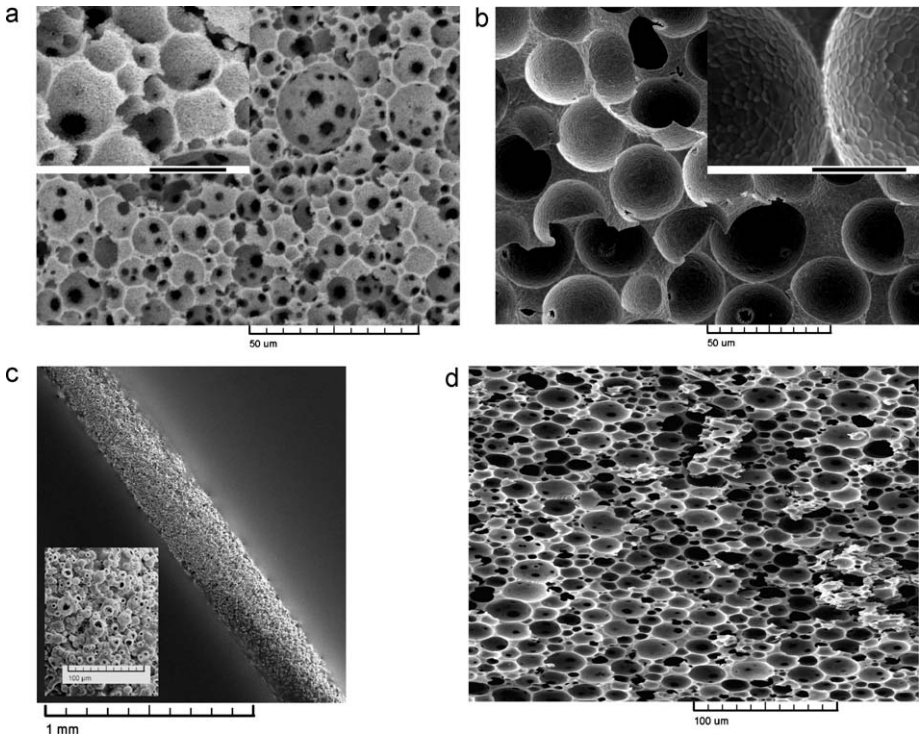

Fig. 6. Cellular articles produced with UV curable dispersions containing solid pore formers. (a) section of a cellular Al_2O_3 disk sintered at 1500 °C with 79% porosity made using PE pore former with a size distribution between 3 and 25 μm, (b) section of a cellular Al_2O_3 disk sintered at 1500 °C with 72% porosity made using monosized 40 μm PS pore former, (c) cellular Al_2O_3 fiber sintered at 1500 °C with 67% porosity made using the PE pore former of example (a), (d) section of a cellular TiO_2 disk debinded at 550 °C with 79% porosity made using the PE pore former of example (a). Scale bars in inserts are 10 μm, unless noted.

by the use of multifunctional monomers and/or curable polymers, is inherent and controllable with UV curable resins. Fig. 6b shows a second example of cellular Al_2O_3 material produced by casting and UV curing of 2 cm diameter disks with thickness of a 2–3 mm using 40 μm pore forming polystyrene spheres (instead of PE used in Fig. 6a). The material is 72% porous and the shape of the pore former is precisely replicated in the cellular ceramic. Larger multilayer samples (2 cm × 2 cm × 1 cm) consisting of 8 layers of the composition shown in Fig. 6a were also demonstrated. Despite the relatively high content of organic matter (∼50 wt%) these samples have retained their structural integrity during processing and are relatively strong. Fig. 6c shows a cellular Al_2O_3 fiber produced with PE pore forming spheres. The fiber was extruded through a 500 μm die by the method of Fig. 4 with water as a static fluid. Due to the relatively high viscosity of the paste, continuous fibers could also be extruded directly to air. The fiber surface displays mostly closed cells (Fig. 6c, insert) and has 67% porosity, of which 19.5% is impermeable to Hg.

Fig. 6d demonstrates that a cellular TiO_2 material with similarly good replication of the pore former shape and size can be obtained. Similar structures have also been produced from other materials such as nano hydroxyapatite. While the cellular Al_2O_3 materials described in Fig. 6 have been sintered at 1500 °C, the cellular TiO_2 material shown in Fig. 6d is only debinded at 550 °C in order to retain its photocatalytic properties. BET and XRD analysis show that the surface area and crystalline phases of the raw powder are retained after the dispersion, shaping and debinding procedures.

The thermal decomposition and phase transformation of $Fe(C_2O_4)\cdot 2H_2O$ raw powder and $Fe(C_2O_4)\cdot 2H_2O$/polyacrylate cured green sheets are shown in Fig. 7a and b, respectively. The raw powder loses 55% of its original weight below 300 °C (Fig. 7a) consistent with the transformation to α-Fe_2O_3. It appears that the decomposition of the oxalate is delayed in the cured sheets, which show an additional weight loss due to polymer burn out, corresponding to the original concentration of oxalate in the dispersions (50 wt%). No major differences between the TGA curves of the commercial and 4-HBA/PEGDA binders can be seen. XRD measurements indicate that the raw oxalate powder has the structure of humboltine. After debinding at 550 °C, both binder systems transform to α-Fe_2O_3 (Fig. 7b). The surface area of the materials after debinding is 27–28 m^2/g indicating formation of primary particles in the range of 40–43 nm (assuming spherical morphology).

Fig. 8 compares cellular α-Fe_2O_3 materials prepared in three different ways. Fig. 8a shows a cellular material derived from α-Fe_2O_3 nanoparticle dispersions in 4-HBA/PEGDA (14:1) monomer mixture. The dispersion was thermally cured at 85 °C for 15 min, debinded at 550 °C and partially sintered at 850 °C for 1 h. The resulting bodies have retained structural integrity but are not fully sintered. After the partial sintering, the hematite phase remains stable but the surface area is reduced from 23.9 to 4.4 m^2/g. As shown also in Fig. 6, the use of nanoparticles (or in other words maintaining high ratio of pore former to particle volume) leads to excellent replication of the 10 μm PMMA pore former. One drawback of the thermal curing employed here is the strong, Arrhenius like dependence of dispersion viscosity on

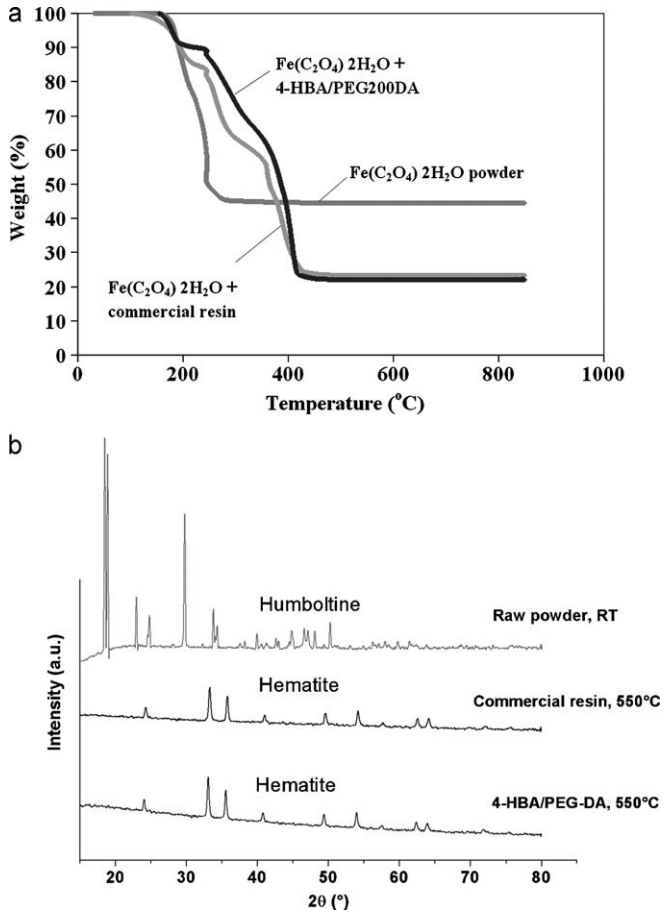

Fig. 7. (a) TGA of $Fe(C_2O_4)\cdot 2H_2O$ raw powder and $Fe(C_2O_4)\cdot 2H_2O$/polyacrylate composite sheets, (b) XRD of $Fe(C_2O_4)\cdot 2H_2O$ raw powder (humboltine) and inorganic sheets obtained after debinding of $Fe(C_2O_4)\cdot 2H_2O$/polyacrylate composites for 2 h at 550 °C in air.

temperature.[10] The dispersion containing pore formers, which was shaped at relatively high viscosity at room temperature is heated to curing temperature (85–90 °C) where the dispersion viscosity may be an order of magnitude lower. At relatively low filling levels (50% nominal porosity), the relatively low density pore formers (0.92–1.2 g/cm^3) may have sufficient time to migrate to the upper surface of the sample before full curing is achieved. Indeed, the lower part of the sample shown in Fig. 8a has a zone where no cells could be observed (not shown here). Fig. 8b and c shows cellular materials derived from the two $Fe(C_2O_4)\cdot 2H_2O$ resin systems by shaping and UV curing of thin sheets. Due to the larger particle size, its anisotropic shape, and (to a lower extent) the thermal decomposition of the salt, the pore former shape is not precisely replicated in the debinded materials. The rod like particles seen in Fig. 8c are due to relatively low degree of comminution of the coarse $Fe(C_2O_4)\cdot 2H_2O$ powder during milling in the higher viscosity commercial resin. Better replication is seen with the 4-HBA/PEGDA (14:1) monomer mixture (Fig. 8b) where the $Fe(C_2O_4)\cdot 2H_2O$ has an average particle size of 1 μm (compared to 6 μm seen with the commercial resin). Note however, that the particle size is only used here as a rough guide since the particles are highly anisotropic. As suggested by Fig. 8a, replication can be significantly improved if the particle size is reduced to the sub micrometer range with additional milling, likely reducing the particle anisotropy at the same time.

3.4. Fabrication of Al_2O_3 microspheres

Microspherical droplets of the low viscosity radiation curable dispersions readily form in a suitable emulsification medium under mild energy mixing conditions. Formation of stable microspheres requires a proper choice of monomer mixture and emulsification medium. The emulsification medium should also have sufficient optical transparency in the UV–vis spectrum to allow UV curing. The droplets in the emulsion such formed can then be rapidly cured to solid microspheres under flow or static conditions. Fig. 9 shows Al_2O_3 microspheres produced by emulsification of a 41.5 vol% Al_2O_3 dispersion in 2-HEA/PEGDA (14:1) with a large quantity of oil and curing under static conditions. The dispersions were stabilized with hydrophilic comb-polyelectrolye surfactants, thus, the mechanism of microsphere droplet formation/stabilization is not likely to involve particle stabilized emulsions such as those proposed by Gonzenbach et al.[17] The cured nanocomposite microspheres were debinded and sintered at 1500 °C to smooth ceramic microspheres with an average size of ∼30 μm but with a relatively wide size distribution. Microspheres as small as

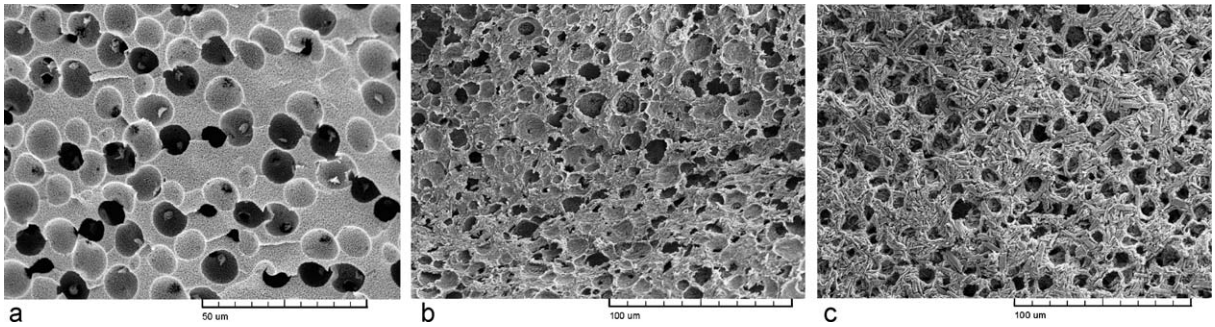

Fig. 8. α-Fe_2O_3 cellular materials with 50% porosity (nominal) made using 10 μm PMMA pore formers. (a) derived from α-Fe_2O_3 nanoparticle dispersions in 4-HBA/PEGDA (14:1) monomer mixture, thermally cured at 90 °C for 30 min and partially sintered at 850 °C, (b) derived from $Fe(C_2O_4)\cdot 2H_2O$ dispersions in 4-HBA/PEGDA (14:1) monomer mixture, UV cured, debinded at 550 °C, (c) derived from $Fe(C_2O_4)\cdot 2H_2O$ dispersions in commercial resin, UV cured, debinded at 550 °C.

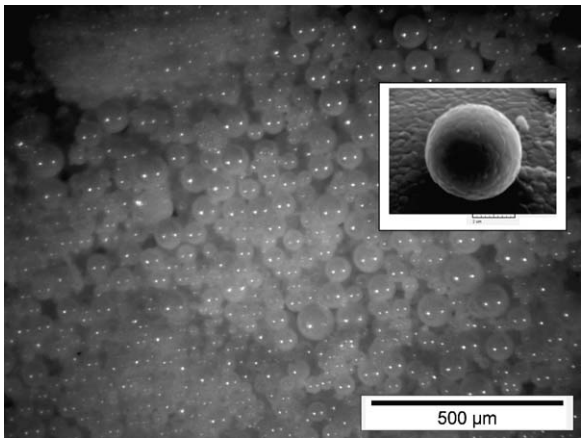

Fig. 9. Al_2O_3 microspheres prepared by emulsification of a 41.5 vol% Al_2O_3 dispersion in 2-HEA/PEGDA (14:1) with oil and rapid UV curing. The spheres were sintered at 1500 °C.

5 μm can easily be produced by this emulsification method (insert, Fig. 9).

4. Conclusions

Dispersions of TiO_2 and α-Fe_2O_3 functional nanoparticles in solvent free, UV curable media with solid loading of 17–19 vol% and viscosity below 0.3 Pa s have been produced with the aid of comb-polyelectrolyte surfactants; demonstrating the generality of this stabilization principle. Colloidal dispersions of metal salts such as $Fe(C_2O_4)\cdot 2H_2O$ in UV curable organic medium with solid loading of 32–33 vol% have similarly been demonstrated. Continuous TiO_2/polyacrylate fibers with dimensions below 10 μm have been produced by spinning and UV curing 'on the fly. α-Fe_2O_3 dispersions could not be cured with medium intensity UV radiation lab equipment. Nevertheless, α-Fe_2O_3 fibers could be produced by spinning of UV curable $Fe(C_2O_4)\cdot 2H_2O$ dispersions into continuous $Fe(C_2O_4)\cdot 2H_2O$/polyacrylate fibers which transform to α-Fe_2O_3 fibers below 550 °C.

New, general and versatile technologies for the fabrication of functional ceramic/polymer cellular articles and microspheres have been developed and demonstrated for α-Al_2O_3 as a model particle, as well as for TiO_2 and α-Fe_2O_3. The solvent free, low viscosity UV curable colloidal dispersions can be loaded with a high amount of pore formers and cured in the shape of fibers, single and multilayered articles. Highly porous cellular ceramics with porosity approaching 80% with controlled cell size and shape in the micrometer range are obtained after conventional debinding and sintering procedures. The replication of pore formers with size <10 μm to fabricate cellular articles is preferred with nanoparticle dispersions. The microshaping techniques described above can be applied to a wide range of materials and structures.

Acknowledgements

The authors would like to thank Dr. Kasia Michalow, Empa, for the help with the photocatalytic experiments.

References

1. Licciulli A, Esposito Corcione C, Greco A, Amicarelli V, Maffezzoli A. Laser stereolithography of ZrO_2 toughened Al_2O_3. *J Eur Ceram Soc* 2005;**25**:1581–9.
2. Halloran JW, Griffith M, Chu T, Stereolithography resin for rapid prototyping of ceramics and metals, US Patent 6117612, 2000.
3. Esposito Corcione C, Greco A, Montagna F, Licciulli A, Maffezzoli A. Silica moulds built by stereolithography. *J Mater Sci* 2005;**40**:4899–904.
4. Dufaud O, Marchal P, Corbel S. Rheological properties of PZT suspensions for stereolithography. *J Eur Ceram Soc* 2002;**22**:2081–92.
5. Jang JH, Wang S, Pilgrim SM, Schulze WA. Preparation and characterization of barium titanate suspensions for stereolithography. *J Am Ceram Soc* 2000;**83**:1804–6.
6. Wu KC, Halloran JW. Photopolymerization monitoring of ceramic stereolithography resins by FTIR methods. *J Mater Sci* 2005;**40**:71–6.
7. Chartier T, Duterte C, Delhote N, Baillargeat D, Verdeyme S, Delage C, Chaput C. Fabrication of millimeter wave components via ceramic stereo- and microstereolithography processes. *J Am Ceram Soc* 2008;**91**:2469–74.
8. Hanemann T, Honnef K, Hausselt J. Process chain development for the rapid prototyping of microstructured polymer, ceramic and metal parts: composite flow behaviour optimisation, replication via reaction moulding and thermal post processing. *Int J Adv Manuf Technol* 2007;**33**:167–75.
9. Brady GA, Halloran JW. Differential photo-calorimetry of photopolymerizable ceramic suspensions. *J Mater Sci* 1998;**33**:4551–60.
10. de Hazan Y, Heinecke J, Weber A, Graule T. High solids loading ceramic colloidal dispersions in UV curable media via comb-polyelectrolyte surfactants. *J Colloid Interface Sci* 2009;**337**:66–74.
11. de Hazan Y, Graule T, Müller G, Process and device for manufacturing shaped composite, the shaped composite and the shaped inorganic article derived from it, patent application WO/2010/040243.
12. de Hazan Y, Wozniak M, Heinecke J, Müller G, Graule T. New microshaping concepts for ceramic/polymer nanocomposite and nanoceramic fibers. *J Am Ceram Soc* 2010;**93**:2456–9.
13. Sepulveda P, Binner JPG. Processing of cellular ceramics by foaming and in situ polymerisation of organic monomers. *J Eur Ceram Soc* 1999;**19**:2059–66.
14. Grader GS, de Hazan Y, Shter GE. Novel ceramic foams from crystals of $AlCl_3(Pr^i{}_2O)$ complex. *J Mater Res* 1999;**14**:1485–94.
15. Scheffler M, Colombo P. *Cellular ceramics*. Weinheim: Wiley-VCH; 2005.
16. Colombo P. Conventional and novel processing methods for cellular ceramics. *Phil Trans R Soc A* 2006;**364**:109–24.
17. Gonzenbach UT, Studart AR, Steinlin D, Tervoort E, Gauckler LJ. Processing of particle-stabilized wet foams into porous ceramics. *J Am Ceram Soc* 2007;**90**:3407–14.
18. Andersson L, Bergström L. Gas-filled microspheres as an expandable sacrificial template for direct casting of complex-shaped macroporous ceramics. *J Eur Ceram Soc* 2007;**28**:2815–21.
19. Akartuna I, Studart AR, Tervoort E, Gauckler LJ. Macroporous ceramics from particle-stabilized emulsions. *Adv Mater* 2008;**20**:4714–8.
20. Barg S, de Moraes EG, Koch D, Grathwohl G. New cellular ceramics from high alkane phase emulsified suspensions (HAPES). *J Eur Ceram Soc* 2009;**29**:2439–46.
21. de Hazan Y, Graule T, Heinecke J, Shaped cellular articles and (micro)spheres, Patent Application WO/2010/124402.
22. Wozniak M, Graule T, de Hazan Y, Kata D, Lis J. Highly loaded UV curable nanosilica dispersions for rapid prototyping applications. *J Eur Ceram Soc* 2009;**29**:2259–65.
23. de Hazan Y, Reuter T, Werner D, Clasen R, Graule T. Interactions and dispersion stability of aluminum oxide colloidal particles in electroless nickel solutions in the presence of comb polyelectrolytes. *J Colloid Interface Sci* 2008;**323**:293–300.
24. Jeong W, Kim J, Kim S, Lee S, Mensing G, Beebe DJ. Hydrodynamic microfabrication via "on the fly" photopolymerization of microscale fibers and tubes. *Lab Chip* 2004;**4**:576–80.
25. Utada AS, Fernandez-Nieves A, Stone HA, Weitz DA. Dripping to jetting transitions in coflowing liquid streams. *Phys Rev Lett* 2007;**99**:094502.

26. Griffith ML, Halloran JW. Scattering of ultraviolet radiation in turbid suspensions. *J Appl Phys* 1997;**81**:2538–46.
27. Wu KC, Seefeldt KF, Solomon MJ, Halloran JW. Prediction of ceramic stereolithography resin sensitivity from theory and measurement of diffusive photon transport. *J Appl Phys* 2005;**98**, 024902+10.
28. Cornell RM, Schwertmann U. *The iron oxides*. Weinheim, Germany: VCH Verlagsgesellschaft mbH; 1996.
29. Angermann A, Töpfer J. Synthesis of magnetite nanoparticles by thermal decomposition of ferrous oxalate dehydrate. *J Mater Sci* 2008;**43**: 5123–30.